Commun. Comput. Phys.
doi: 10.4208/cicp.130410.031210a

Vol. **10**, No. 4, pp. 920-939
October 2011

A Kinetic Monte Carlo Approach for Self-Diffusion of Pt Atom Clusters on a Pt(111) Surface

R. Deák[1,2], Z. Néda[1,*] and P. B. Barna[3]

[1] *Department of Theoretical and Computational Physics, Babeş-Bolyai University, RO-400084, Cluj-Napoca, Romania.*
[2] *Department of Materials Physics, Eötvös Loránd University, H-1117, Budapest, Hungary.*
[3] *KFKI-MFA, Research Institute for Technical Physics and Materials Science, H-1525, Budapest, Hungary.*

Received 13 April 2010; Accepted (in revised version) 3 December 2010

Communicated by Leonardo Golubovic

Available online 13 June 2011

Abstract. A lattice Kinetic Monte Carlo (KMC) approach is considered to study the statistical properties of the diffusion of Pt atom clusters on a Pt(111) surface. The interatomic potential experienced by the diffusing atoms is calculated by the embedded atom method and the hopping barrier for the allowed atomic movements are calculated using the Nudged Elastic Band method. The diffusion coefficient is computed for various cluster sizes and system temperatures. The obtained results are in agreement with the ones obtained in previous experimental and theoretical works. A simple scaling argument is proposed for the size dependence of the diffusion coefficient's prefactor. A detailed statistical analysis of the event by event KMC dynamics reveals two important and co-existing mechanisms for the diffusion of the cluster's center of mass. At low temperatures (below $T=400$K) the dominating mechanism responsible for the displacement of the cluster's center of mass is the periphery (or edge) diffusion of the atoms. At high temperatures (above $T=800$K) the dissociation and recombination of the clusters becomes more and more important.

PACS: 05.10.-a, 68.35.Fx, 68.43.Jk
Key words: Kinetic Monte Carlo methods, surface diffusion, diffusion coefficient.

1 Introduction

Understanding surface diffusion of single adatoms and small adatom clusters is an important step for realistic modeling of various phenomena related to thin film growth: island nucleation, island coalescence and Ostwald ripening [1]. Over the years experimental techniques, like scanning tunneling microscopy (STM) [2,3] and Field Ion Microscopy

*Corresponding author. *Email address:* zneda@phys.ubbcluj.ro (Z. Néda)

(FIM) [4–7] was used to obtain precious insight into this phenomena. Experimental observations were completed by several theoretical methods like static calculations [8–10], molecular dynamics (MD) [11,12] and Monte Carlo methods (MC) [13,14]. In the present work a Kinetic Monte Carlo (KMC) approach is considered to study the diffusion coefficient of single Pt atoms and clusters on Pt(111) surface.

It is a well-known fact that MC simulations are less accurate approximation to reality than the nowadays fashionable *ab*-initio Molecular Dynamics methods (for a review see [15]). The advantage of the *ab*-initio methods is that they do not rely on phenomenological interaction potentials but calculate them from first-principles. *Ab*-inito MD simulations provide an accurate description of inter-atomic interactions, but naturally there is price to pay for this. The price is the extremely long computational time. Therefore *ab*-initio methods are restricted to relatively small systems and short simulation times. The very short time-scale which is manageable on modern supercomputers (of the order of nano-seconds) makes these methods inappropriate for studying the diffusion coefficient of the surface diffusion. In contrast to MD methods, in KMC simulations several processes are taken into account in a phenomenological manner, many times without a microscopic foundation. The interaction potentials governing the dynamics of the atoms and consecutively the values of energy barriers for the particle moves are either heuristic ones or approximated from Density Functional Theory (DFT) calculations [16]. MC simulations offer, however, a great advantage (for a review see [17]): it is fast and one can study thus larger systems and much longer time-scales. Due to these advantages the method is more adaptable for moderate computational resources than MD methods. With KMC methods a quite reasonable number of atoms can be studied on cheap PC type computers. MD methods and MC methods are complementing thus each other. Parallel with developing fast and realistic MD methods, making the KMC simulations more realistic is also an important task. KMC simulations are nowadays targeting structures on mesoscopic scale or complex phenomena that has characteristic time-scale of the order of seconds or larger. Since the characteristic time-scale for the diffusion of adatom clusters on a crystalline surface is much larger than the time-scales manageable by MD methods we have chosen to consider an up to date KMC method.

The present paper is structured as follows. In Section 2 we describe briefly the main elements of the KMC method and how the method is implemented for the specific problem considered in the present work. In Section 3 we discuss some theoretical arguments regarding the diffusion coefficient and its variation as a function of temperature and cluster size. KMC simulation results are presented and discussed in Section 4. Section 5 is devoted to general conclusions.

2 The KMC approach and computational details

2.1 The KMC method, a brief review

Kinetic (sometimes labeled as resident-time, or BKL-type) Monte Carlo methods [18] are appropriate for simulating those dynamical phenomena where several processes with

widely different time-scales are simultaneously present. For epitaxial thin-film growth this is the case since: (i) atoms can be deposited on a crystalline surface with a given rate; (ii) atoms can diffuse on the surface governed by different rates which depends on the binding energy of the specific location of the atom; (iii) Decohesion of adatoms from the surface with a given rate can occur. The main idea of the KMC simulation method is that in each simulation step one process is probabilistically selected (with probability proportional with its rate) and carried out. The time is updated then non-uniformly and non-deterministically, depending on the rates of all possible processes at that given moment [18]. For thin-film growth simulations usually, the *deposition (adsorption) rate* is fixed and calculated from the deposition speed (deposition flux) given as the number of new monolayers deposited in unit time (ML/s). The *diffusion rate* ($r_{X\to Y}$) of an atom is governed by the thermodynamic temperature (T) of the system and the potential barrier ($\Delta E_{X\to Y}$) that the atom has to overcome between the initial (X) and the final (Y) position:

$$r_{X\to Y} = f_0 \exp\Big(-\frac{\Delta E_{X\to Y}}{k_B T}\Big). \tag{2.1}$$

In expression (2.1) k_B is the Boltzmann factor and f_0 is the attempt rate, which is roughly the vibration frequency of atoms in the crystal ($f_0 \sim 10^{12}$Hz). Since the value of the barrier is not straightforward to estimate (even if the pair-interaction potential between the atoms is known), several simplifying methods are used [19–22]. The simplest approach is to consider the potential barrier dependent only on the binding energy of the atom in the initial (X) state [21, 23] or by applying the transition state theory [24]. A better, but computationally more costly approach is to consider a realistic interatomic potential and estimate the potential in several points between the initial and final state. In such case the difference between the maximum and initial value along the minimum energy path will yield the potential barrier. There are several techniques known in the literature for finding the saddle point. The most well-known ones are the Nudged Elastic Band (NEB) [25, 26] and the Dimer method [27]. In order to apply these methods, one has to determine first the potential energy landscape in several points. The Embedded Atom Method (EAM) [28–30] offers a good and reliable method for this. Nowadays, with the advances in *ab*-initio methods, DFT calculations can be also successfully applied to estimate the energy landscape [16, 22, 31].

The *desorption rate* can be obtained either by fixing a phenomenological potential barrier E_{dec} for this process or by calculating the more realistic potential barrier from first principles, as the binding energy of the chosen atom at the given site. Simulations are usually performed in a two-dimensional geometry [21, 23], the atoms being allowed to occupy the sites of a pre-defined lattice. By this approach one reproduces an idealized situation where a new layer is growing on a perfect crystalline substrate. The simplest possibility is to consider a square lattice and the sites on the growing layer positioned exactly on the top of the atoms forming the substrate [21, 23]. In such manner a non-realistic three-dimensional cubic structure is simulated but approaches on more complex geometries are also possible. One can use lattices with different symmetries and different

stacking sequences for positioning the atoms in the growing layer [17, 22, 31]. Simulations can be made more realistic by considering a second "buffer" layer on the top of the simulated one so that interchanges between these two layers become also possible. This allows the formation of additional defects and vacancies [19, 20]. Nowadays computationally costly off-lattice kinetic Monte Carlo methods [32, 33] are also considered for the case when several types of atoms are simultaneously present and therefore it is a lattice constant or symmetry mismatch between the crystalline structures of the components. In such an approach the allowed positions of the atoms are not exclusively the sites of a crystalline lattice, like in lattice kinetic Monte Carlo methods, but are computed from an energy minimization procedure and the dynamics of the system is realized with the kinetic Monte Carlo algorithm.

2.2 The present approach

In the present work we investigate the diffusion of the Pt atoms and clusters on a Pt(111) surface. This particular system was explicitly chosen because Pt is one of the most studied materials in thin film growth, several experimental results and *ab*-initio calculations are available, allowing to verify the simulation results in special cases.

For calculating the potentials experienced by the diffusing atoms the generalized EAM potential is used. The hopping barrier is determined by the NEB method. A single-atom diffusion mechanism is considered neglecting the concerted and simultaneous moves of several atoms from the cluster. These concerted moves would lead to several complications in applying the NEB method and would increase strongly the necessary computation time. However, as discussed for Cu clusters on Cu(111) surfaces in [34], neglecting the collective motion of atoms might lead to unrealistically small diffusion constant values (and thus unrealistically high diffusion barriers) in the case of small stable cluster configurations like trimers and heptamers. Our results will definitely suffer of this deficiency, however in case of Pt clusters diffusion on Pt(111) surfaces this effect is expected to be much smaller due to the stronger interatomic potentials and much higher effective barriers values. For example, for Cu monomers on Cu(111) surfaces experiments [34] gives $E_m = 37 \pm 5$meV, while for Pt monomers on Pt(111) surface experiments [6] indicate $E_m = 260$meV, a value which is one order of magnitude higher. This huge difference is due to the stronger interatomic potential which decreases also the probability of collective motion of the atoms.

For single atom moves all the relevant degrees of freedom for diffusion are taken into account, so we believe that the considered approach is a realistic one. As substrate a triangular lattice ((111) plane of the FCC structure) is used and atoms are considered as spheres. The topology of the substrate atoms is sketch with filled circles in Fig. 1. In such manner, there are two triangular sub-lattices (empty circles and crosses in Fig. 1) on which the adatoms can be deposited and diffuse, forming monolayer lattices of FCC and HCP crystalline phases. Due to geometric restrictions atoms in the growing layer cannot occupy neighboring sites belonging to different sub-lattices. Considering a bulk FCC

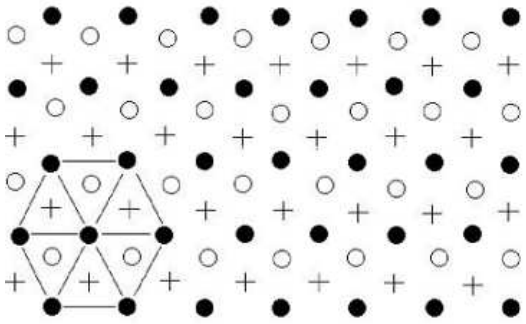

Figure 1: Geometry of the considered lattice. Filled circles represents the sites of the substrate, empty circles and crosses represents the FCC and HCP lattice sites, respectively.

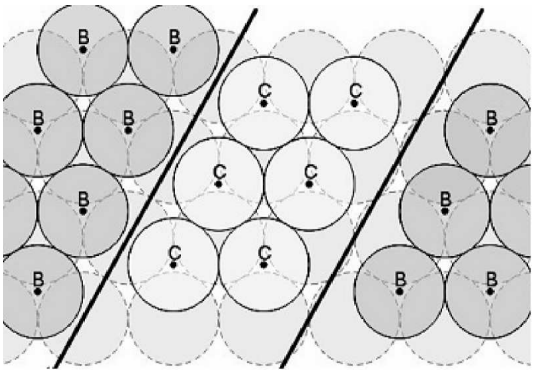

Figure 2: Phase-boundaries that can be formed on the triangular FCC surface.

substrate, stacking fault develops at the interface of the substrate and a growing HCP monolayer island (Fig. 2). By this manner phase boundaries can also appear between growing islands of FCC and HCP types.

The edge of the cubes in the Pt FCC structure is 3.92×10^{-10}m [35] which yields 2.77×10^{-10}m as lattice constant for the considered triangular lattice substrate. From experiments it is also known that the energy barrier for a free Pt atom jumping on the sites of the (111) plane of the FCC lattice (sometimes called activation energy or migration energy (E_m)) is around 0.25-0.26eV [6, 11, 22]. The attempt frequency is taken as $k_0 = 5\times10^{12}$Hz, the order of magnitude that is generally assumed for the vibration frequency of atoms.

In agreement with earlier studies [19, 20] we assume two possible mechanisms for cluster diffusion (shown in Fig. 3):

a) Diffusion of atoms on the cluster edge (periphery diffusion).

b) Dissociation of the cluster in two parts, which can diffuse by their own, and recombine in a cluster with the original size.

In order to avoid the interaction and mixing between clusters, systems containing

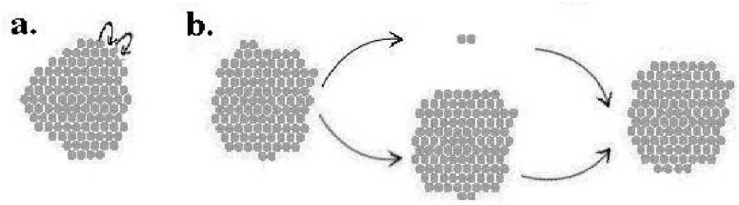

Figure 3: Two mechanisms for cluster diffusion: a) edge diffusion of atoms around the cluster and b) dissociation of the cluster into two diffusing clusters that recombine into a cluster with the original size.

initially just one cluster are considered. During simulation this cluster might fragment in parts, and the simulation is stopped whenever the biggest component becomes smaller than 90% of the original size. Clusters with sizes $N=1,2,3,4,5,6,7,9,13,19,25,30$ and 37 atoms are studied. As starting configurations a densely packed structure (as close as possible to disc-shape form) is considered. During simulation no addition deposition of atoms are considered ($F=0$Ml/s) and various temperatures ranging from 300K to 900K are fixed. The simulated lattice size is 256×256 and periodic boundary conditions are imposed. Three consecutive and fixed layers of substrate atoms are considered.

2.3 The energy barrier calculation method

The NEB method [25, 26] is used for finding the Minimum Energy Path (MEP) of the diffusing atoms. NEB is an efficient method to determine the saddle points (and consecutively the energy barrier) between a given initial and final state of a transition. The method uses a number of replicas (images) of the diffusing atom, displaced along a continuous path between the initial and final state of a diffusion step. These replicas are coupled with fictitious springs to ensure continuity of the path, therefore each of them feels forces due to external potential and the coupled springs. The basic idea of NEB is that the elastic forces are projected along the path and the external forces are projected orthogonally to the path. The relaxing force of the i-th image is:

$$\begin{aligned}\vec{F}_i^{rel} &= -\nabla V(\vec{R}_i)_\perp + \left(\vec{F}_i^{spring}\right)\big|_\parallel \\ &= -\nabla V(\vec{R}_i) + \left[\nabla V(\vec{R}_i)\cdot\hat{\tau}_i\right]\hat{\tau}_i + \left[k(\vec{R}_{i+1}+\vec{R}_{i-1}-2\vec{R}_i)\cdot\hat{\tau}_i\right]\hat{\tau}_i,\end{aligned} \tag{2.2}$$

where $\vec{R}_i$ is the coordinate vector of the i-th image, $V(\vec{R}_i)$ is the interaction potential felt by the hopping system and $\vec{F}_i^{spring}$ is the spring force acting on the image. k is the spring constant and $\hat{\tau}_i=\vec{\tau}_i/|\tau_i|$ is the normalized tangent vector along the MEP and at the location of the i-th image.

The initial coordinates of the images are calculated using a simple linear interpolation between the initial and final point, after that the band is optimized to reach the MEP using the steepest descent method. The energy barrier of the transition is the difference between two consecutive potential energy minimum and maximum along the oriented MEP. This energy difference is referenced from now on as the height of the saddle point.

When multiple saddle points are detected, the barrier is given as the sum of the saddle points height. Multiple saddle points are in cases when the MEP contain an intermediate lattice site, for example: in case of an FCC-FCC jump intermediate minimum could be a neighboring HCP site. In the present simulations the adjustable spring-constant parameter was chosen as $k=0.65\text{eV}/\text{Å}$ and 19 replicas were considered along the band.

2.4 Interatomic potential

The generalized EAM [29, 30] was used to calculate the interatomic potentials. This potential has been already used with success to simulate both bulk and surface properties of multilayer films [30]. EAM offers a realistic many-body approach, where the potential energy of an atom i is a sum of two terms:

$$U_i=\sum_{j\neq i}\phi(r_{ij})+F(\rho_i). \tag{2.3}$$

The first term represents the simple pair-interaction energy between the i-th and all the other j-th atoms, the second term is the many-body term resulting from the interaction of the embed i atom with the local-electron density provided by the other atoms. The pair potentials are calculated [29] by the following equation

$$\phi(r_{ij})=\frac{A\cdot\exp\left[-\alpha\left(\frac{r_{ij}}{r_e}-1\right)\right]}{1+\left(\frac{r_{ij}}{r_e}-\kappa\right)^{20}}-\frac{B\cdot\exp\left[-\beta\left(\frac{r_{ij}}{r_e}-1\right)\right]}{1+\left(\frac{r_{ij}}{r_e}-\lambda\right)^{20}}, \tag{2.4}$$

where r_e is the equilibrium distance between nearest neighboring atoms. A, B, α, β, κ and λ are adjustable parameters of the potential.

The embedding energy term can be determined as follows [30]:

$$F(\rho_i)=\begin{cases}\sum_{x=0}^{3}F_{nx}\left(\frac{\rho_i}{\rho_n}-1\right)^x, & \text{if } \rho_i<\rho_n,\ \rho_n=0.85\rho_e,\\ \sum_{x=0}^{3}F_x\left(\frac{\rho_i}{\rho_n}-1\right)^x, & \text{if } \rho_n\leq\rho_i<\rho_0,\ \rho_0=1.15\rho_e,\\ F_e\left[1-\ln\left(\frac{\rho_i}{\rho_e}\right)^\eta\right]\cdot\left(\frac{\rho}{\rho_e}\right)^\eta, & \text{if } \rho_0\leq\rho_i.\end{cases} \tag{2.5}$$

The value of ρ_i is given by

$$\rho_i=\sum_{j\neq i}f_j(r_{ij}), \tag{2.6}$$

where $f_j(r_{ij})$ is the electron density created by atom j at the coordinate of atom i, and can be written as:

$$f_j(r_{ij})=\frac{f_e\cdot\exp\left[-\beta\left(\frac{r_{ij}}{r_e}-1\right)\right]}{1+\left(\frac{r_{ij}}{r_e}-\lambda\right)^{20}}. \tag{2.7}$$

Table 1: EAM parameters for Pt. Values are given here with three decimal precision. For the more exact values please consult [30].

r_e (Å)	2.772	F_{n0} (eV)	-4.010
f_e (eV/Å)	2.337	F_{n1} (eV)	-0.755
ρ_e (eV/Å)	34.109	F_{n2} (eV)	1.767
α	7.080	F_{n3} (eV)	-1.578
β	3.776	F_0 (eV)	-4.17
A (eV)	0.450	F_1 (eV)	0
B (eV)	0.594	F_2 (eV)	3.475
κ	0.413	F_3 (eV)	2.288
λ	0.827	F_e (eV)	-4.174
η	1.393		

The other parameters involved in the calculation of the EAM potential for Pt (see for example [30]) are listed in Table 1.

3 The diffusion coefficient

Our aim is to compute the value of the diffusion coefficient for various cluster sizes and temperatures. In general, the diffusion coefficient (D) is derived by following as a function of time the mean-square displacement of the cluster's Center of Mass (CM). The mathematical definition of D is

$$D = \frac{\langle (\Delta\vec{r}(t))^2 \rangle}{2d \cdot t}, \tag{3.1}$$

where $(\Delta\vec{r}(t))^2$ is the square of the displacement of the CM in time t and d is the dimensionality of the lattice. The best method to compute D is by plotting $\langle (\Delta\vec{r}(t))^2 \rangle$ as a function of t and determining the slope of the obtained linear dependence. This was also the method used in the present study. The diffusion coefficient exhibits the well-known Arrhenius-like behavior as a function of temperature [36]:

$$D = D_0 \exp\Big(-\frac{E_m}{k_B T}\Big). \tag{3.2}$$

In (3.2), D_0 is the pre-factor of the diffusion coefficient, E_m is a phenomenological activation energy (or sometime called migration energy) of the diffusing particle or cluster, k_B is the Boltzmann constant and T is the thermodynamic temperature of the system. D_0 and E_m can be calculated by studying the diffusion coefficient at different temperatures. One might assume that for clusters of different sizes both D_0 and E_m is dependent as a function of the cluster size, i.e., $D_0 = D_0(N)$ and $E_m = E_m(N)$.

Previously, Voter and Doll [12] considered an MD simulations for studying the diffusion coefficient's, dependence as a function of the cluster size. For clusters containing more than 10 atoms they proposed a power-law dependence.

Several other theoretical studies reported similar behavior, with largely different scaling exponents that depends on the considered material, temperature and model [13, 37–39]. Many of the previous studies have also a critical view on the scaling behavior, emphasizing that the results are rather ambiguous due to the restricted cluster sizes and due to the oversimplified model.

Here, we propose a simple theoretical argument for the size dependence of the D_0 pre-factor when periphery diffusion is the dominant mechanism for the cluster diffusion (Fig. 3(a)). Let us assume a cluster of atoms of size N. Assuming that this cluster is usually a compact disk-like structure (configuration close to the minimum energy configuration), its perimeter is proportional with $N^{1/2}$. The number of atoms capable for periphery diffusion, N_{diff} is thus:

$$N_{diff} \sim N^{\frac{1}{2}}. \tag{3.3}$$

For the problem considered in the present study, our KMC simulations proved that the periphery motion of atoms is indeed the leading mechanism for cluster diffusion. This periphery diffusion is a rapid one, atoms performing several thousands of cycles in unit time. Due to the edge diffusion of one periphery atom, the average displacement, $\langle r_1 \rangle$ of the CM of the cluster of size N in unit time is proportional with the radius, R_N, of the cluster (average displacement length of one atom) and inversely proportional with the total mass of the cluster (N):

$$\langle r_1 \rangle \sim \frac{R_N}{N} \sim N^{-\frac{1}{2}}. \tag{3.4}$$

The pre-factor of the diffusion coefficient, due to the motion of one single periphery atom, D_{01}, is thus:

$$D_{01} \sim \langle r_1 \rangle^2 \sim N^{-1}. \tag{3.5}$$

The pre-factor D_0 is a result of the edge diffusion of all periphery atoms. One might expect:

$$D_0 \sim N_{diff} \cdot D_{01} \sim N^{\frac{1}{2}} \cdot N^{-1} \sim N^{-\frac{1}{2}}. \tag{3.6}$$

One of the aims of the present paper is to prove this simple conjecture.

4 Results and discussion

Lattice KMC simulations for different temperatures and different cluster sizes were performed to investigate the temperature and size dependence of the diffusion of Pt clusters on Pt(111) surfaces. For each cluster size and temperature several runs (of the order of 10) were performed and the obtained results were averaged. The length of one run (number of atomic jumps) was largely different for different cluster sizes. While for monomers 20000 jumps were enough to reach a reasonable distance of the CM relative to the starting position, for larger clusters (for example $N = 37$) around 800,000 individual jumps were necessary. Computational time increased thus very much for large clusters. Calculation of the potentials were parallelized on 6 processors. Simulations were done on a cluster of

88 Xeon Processors, linked by a Myrinet network. Simulation results are discussed in the following.

4.1 Arrhenius behavior

Simulations performed at various temperatures prove the validity of the Arrhenius relation (Eq. (3.2)). Results for $\ln(D)$ as a function of $1/k_BT$ are plotted on Fig. 4. Different curves are for different cluster sizes, as illustrated in the legend. The Arrhenius relation holds for all cluster sizes, although for closed shell clusters (for example $N=7$), the diffusion constant values are lower than expected from the general trend after the cluster sizes.

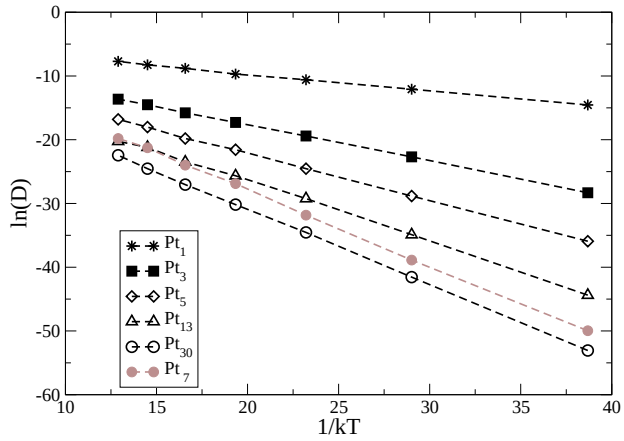

Figure 4: Arrhenius behavior of the diffusion coefficient for several cluster sizes. Note the smaller than expected diffusion constant values for the $N=7$ closed shell clusters.

For single Pt atom diffusion the results indicate $D_0=4.3\times10^{-3}\text{cm}^2/\text{s}$ and $E_m=0.2\text{eV}$ which is in reasonable agreement with the established results form the literature. The values of D_0 and E_m measured from experiments are $2(\times1.4^{\pm1})\times10^{-3}\text{cm}^2/\text{s}$ and $0.26\pm0.03\text{eV}$, respectively [6]. Results of MD simulations using the EAM suggested $D_0=2.41\times10^{-3}\text{cm}^2/\text{s}$ and $E_m=0.19\text{eV}$ [11]. MD studies using Lenard Jones potential yield $D_0=6.3\times10^{-4}\text{cm}^2/\text{s}$ and $E_m=0.19\text{eV}$ [10].

The above results indicates that the average migration energy, E_m, calculated from the Arrhenius relation (Eq. (3.2)) is somewhat smaller than the experimental one. The obtained result is however in agreement with the barrier values expected theoretically using the EAM and NEB. In our KMC simulations, the atoms can diffuse on both stacking (FCC and HCP ones). The diffusion barriers for the jumps of one freely moving atom on same or different stacking are summarized in Table 2.

The average diffusion energy should be thus somewhere between 0.294eV and 0.146eV. Since the HCP-FCC and FCC-HCP jumps are more frequent the obtained E_m value should be closer to the lower bond. The obtained result is in agreement with these requirements.

Table 2: Computed diffusion barriers for a freely moving atom.

$FCC-FCC$	0.293eV
$HCP-HCP$	0.294eV
$FCC-HCP$	0.148eV
$HCP-FCC$	0.146eV

Let us turn our attention now to the diffusion of the clusters ($N>1$). As Fig. 4 indicates the Arrhenius behavior is valid in all cases. The migration energy values calculated for clusters of various sizes are summarized in Fig. 5.

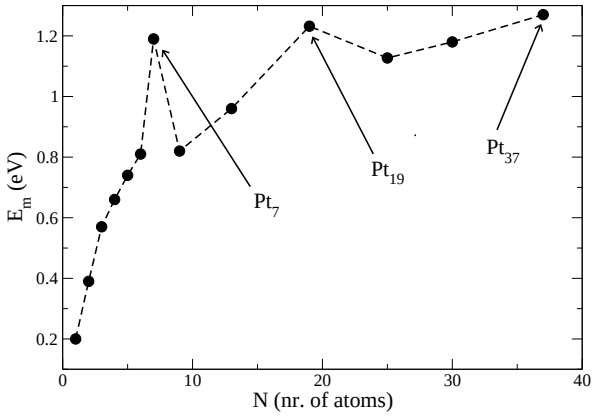

Figure 5: Simulation energy for the migration energy, E_m, for clusters of various sizes, N. Please note the local maximum for close-shell clusters.

These values can be compared with the values determined from FIM experiments [6] and those calculated by the Effective Medium Theory (EMT) for clusters with sizes up to $N=7$ atoms [8]. Results are plotted on Fig. 6(a). From this figure one concludes a fair agreement of our KMC simulation results with the experimental data. The EMT results have a similar trend, but seemingly their agreement with experimental results is less impressive. The values of the D_0 pre-factors are also in good agreement with the FIM experimental results (Fig. 6(b)). A strong difference is obtained for clusters composed by $N=7$ atoms. In this case experiments suggests $D_0=5.1(\times 3.8^{\pm 1})\times 10^{-1}\text{cm}^2/\text{s}$, while our simulations yield $D_0=1.6\times 10^{-2}\text{cm}^2/\text{s}$. The $N=7$ atom clusters are the smallest closed shell clusters on the FCC lattice. As it was emphasized already in Section 2.2 for small close-shell clusters the concerted motion of atoms become important. In the computational approach considered here these were neglected, so it can be assumed that the difference between experimental results and simulations is a result of our single-atom diffusion approximation. Further closed shell structures are the ones containing $N=19$ and $N=37$ atoms. From Fig. 5 we learn that E_m has local maximums in these cases as well. Fig. 5 suggests also the saturating trend of the migration energy as the cluster size increases.

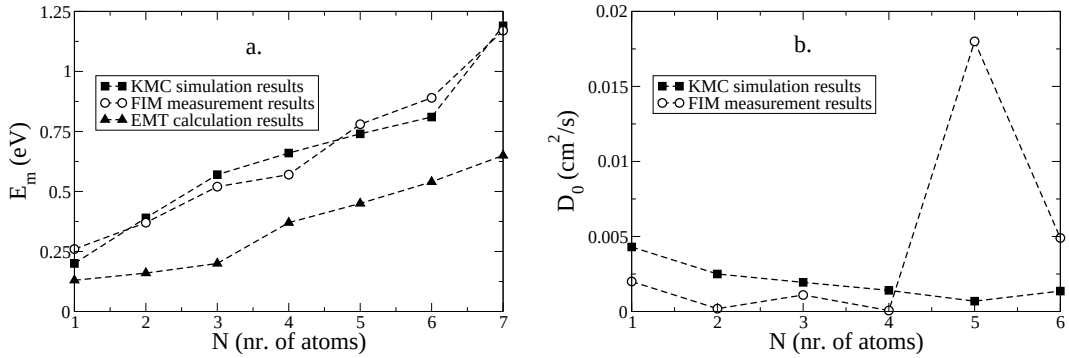

Figure 6: Simulation results for the values of the E_m migration energy (a) and for the D_0 pre-factor of the diffusion coefficient (b) as a function of the cluster size, N.

4.2 Size dependence

Let us turn now the attention on the size dependence of the diffusion coefficient. As discussed in Section 4, one would expect that both D_0 and E_m depends as a function of the cluster size: $D_0 = D_0(N)$ and $E_m = E_m(N)$. Fig. 5 illustrates the trend of the $E_m(N)$ dependence, suggesting a saturating trend for larger clusters. Many earlier numerical studies [12,13,37,38] suggested without any analytical foundation a power-law behavior of $D(N)$ for clusters containing more than 10 atoms. The suggested scaling exponents are widely different and depends both on model and temperature range.

Plotting the diffusion coefficient versus the cluster size on a log-log plot one would expect thus straight lines. For the relatively small clusters considered in our KMC simulations ($N \leq 37$) this conjecture holds relatively well. On Fig. 7(a) we present the $\log(D)$ versus $\log(N)$ plot for several temperatures. If one would force a power-law fit $D = C \cdot N^{\gamma}$ on these curves the results would yield γ scaling exponents that vary strongly with the temperature (Fig. 7(b)). However, due to the very restricted cluster sizes we were able to study with the available computational resources ($N \leq 37$), the power-law claim is not rigorously sustainable.

In Section 3 we presented a simple argument (Eqs. (3.3)-(3.6)) for the scaling property of the D_0 pre-factor: $D_0 \sim N^{-1/2}$. The D_0 values determined from our KMC simulations supports this conjecture. Plotting $\log(D_0)$ as a function of $\log(N)$ for simulations done at various temperatures leads to almost overlapping curves (Fig. 8). The general trends on this log-log plot suggest scaling with an exponent very close to the predicted -0.5 value. On Fig. 8 it is also observable that for the $N = 7$ closed shell configuration a huge peak is present: the pre-factor increases with almost two orders of magnitudes. As we discussed before, the migration energy has also a clear and understandable maximum for $N = 7$ (Fig. 5). This maximum in E_m would decrease the value of the diffusion coefficient. The peak in the pre-factor is however much more puzzling, and will balance in part the effect of E_m. Several previous experimental and simulation studies [4–7,9] noticed this peak in D_0, both for the Pt_7 and Ir_7 clusters. Presently there is no final and conclusive explanation

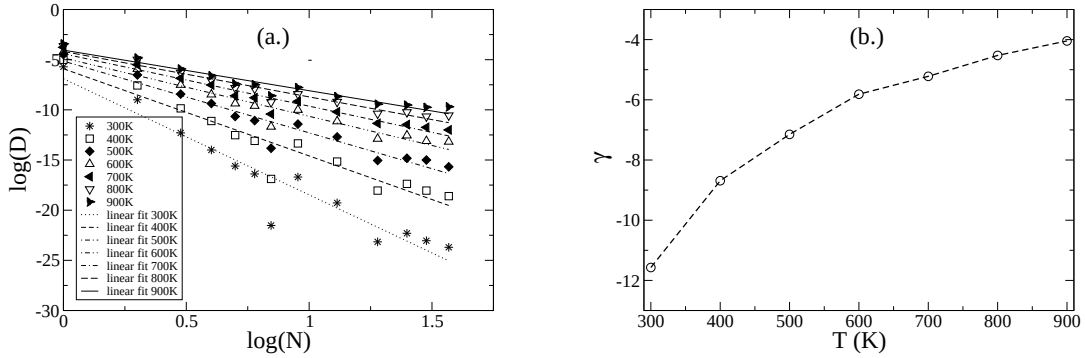

Figure 7: Double logarithmic plot of the cluster size dependence of the diffusion coefficient ($\log(D)$ vs. $\log(N)$). Results for various temperatures and a $D{=}C{\cdot}N^{\gamma}$ power-law fit for the data-points. (b) illustrates the dependence of the γ scaling exponent as a function of temperature.

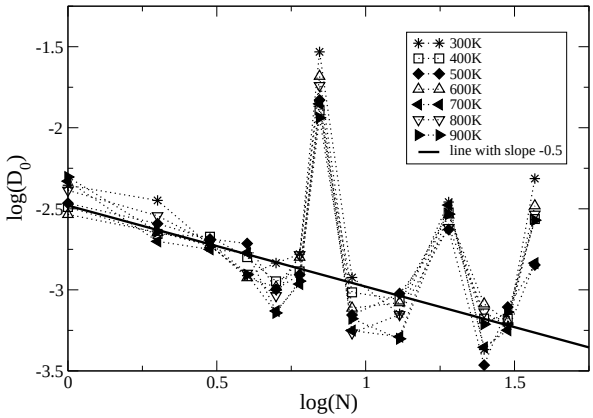

Figure 8: Size dependence of the D_0 pre-factor of the diffusion coefficient.

for its occurrence. Our feeling is that this peak is also an artifact due to the single-atom diffusion approximation considered in our KMC simulations.

4.3 Jump-size statistics

Up to now we described the surface diffusion of the clusters by means of an ensemble averaged phenomenological quantity: the diffusion coefficient. However, computer simulations allow much more! The surface diffusion of the clusters can be approached on an event by event level, analyzing the individual displacements in the clusters CM as well. After each KMC event, one can compute this absolute displacement and their statistics could yield additional information on the diffusion process. Our studies will focus on an open shell cluster: Pt_{13}. In the following we will use simply the term "jump" for the displacement of the CM in one KMC step. The size of these jumps will be measured in lattice constant units.

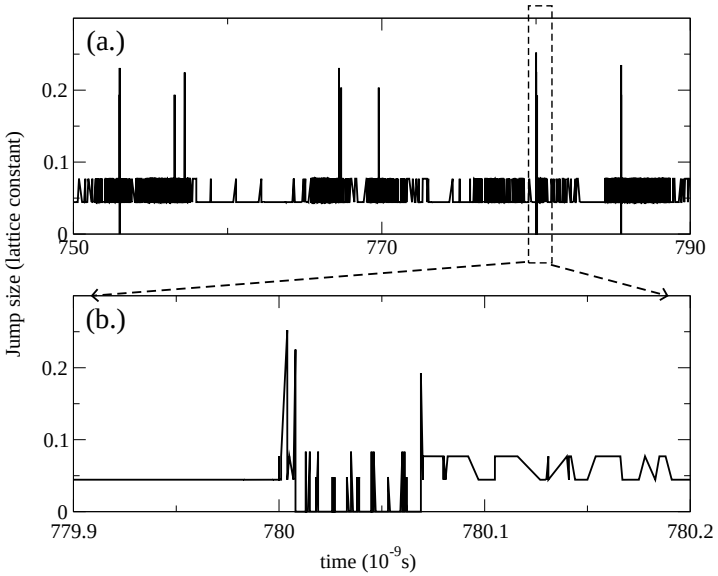

Figure 9: Jumps of the clusters CM as a function of time. (b) is a magnification of a part of (a).

On Fig. 9(a) and Fig. 9(b) results for a simulation performed at $T = 900$K are given plotting the size of the jumps as a function of time. Fig. 9(b) is a magnification of a small part of Fig. 9(a), illustrating the quantized nature of these jumps and the fact that in the KMC simulation time evolves in non-uniform steps.

Jumps of sizes 0 occurs when a freely moving atom (an atom which escaped from the cluster) makes a diffusion step. The CM of the cluster remains immobile in this time period. Jumps smaller than 0.12 lattice constants, are characteristic for edge diffusion. This threshold value can be obtained by simple geometrical considerations, following what happens with the position of the CM when an atom on the edge of a cluster with $N = 13$ moves to a neighboring empty site.

In our model two different types of edge diffusion mechanism are competing Fig. 3. The first one is when an atom from the clusters edge moves between an FCC and HCP site. The second one is when the moving atom remains on the FCC or HCP sub-lattice. In the first case we observe jump sizes smaller than 0.07 lattice-constant, while in the second case we get jump sizes between 0.07 and 0.12 lattice constant.

Whenever an atom leaves a cluster or re-attaches to the cluster, the displacement of the clusters CM changes more drastically than in the case of the diffusion of atoms on the edge of the cluster. The jump sizes are bigger than 0.12 lattice constant in such cases.

It is instructive now to follow the jump size statistics of non-zero jumps at different temperatures. Simulations at 300K, 500K, 700K and 900K were performed. The jump size statistics are presented as simple histograms on Figs. 10(a)-(d). For all studied temperatures the majority of the CM's jumps are around 0.05 lattice constant. In order to visualize the frequency of much less abundant jumps we use a logarithmic scale. These histograms

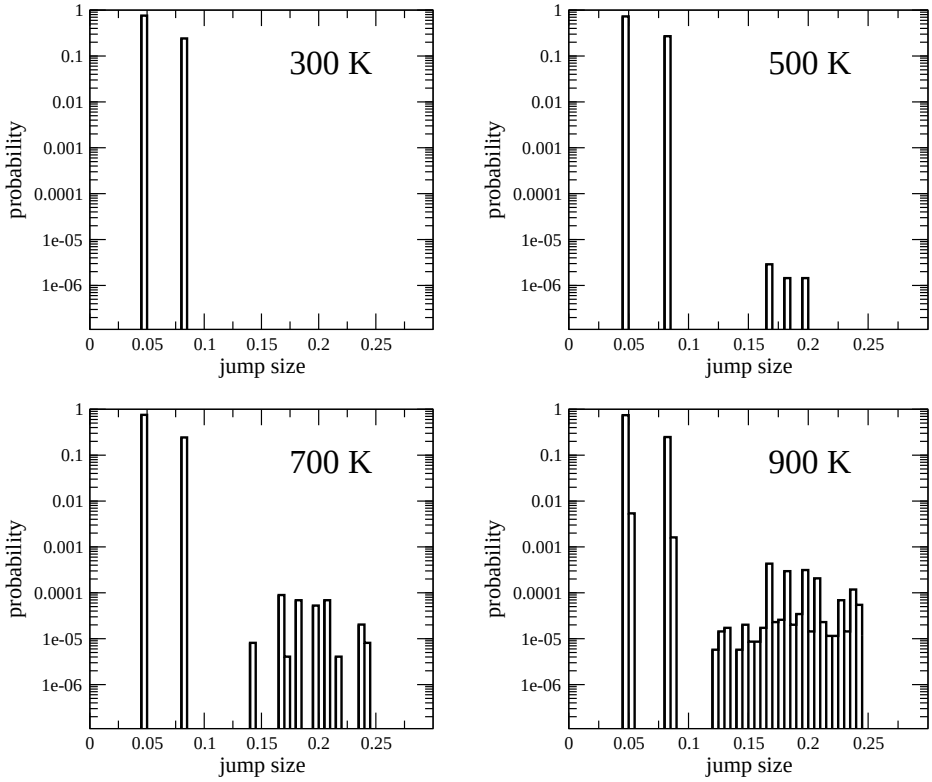

Figure 10: Jump-size statistics (histograms) for different temperatures. Please note the logarithmic vertical scale.

illustrate nicely the effect of temperature on the relative frequency of the main diffusion mechanisms in the model. At lower temperature ($T = 300$K) the edge diffusion mechanism is the leading one, since the jump sizes are mostly below 0.12 lattice constants. As one would naturally expect, for higher temperatures ($T = 700$K and $T = 900$K) the cluster fragmentation probability becomes higher, leading to jumps bigger than 0.12 lattice constants.

Analyzing the statistics of the jump sizes we got the same conclusion as from the analysis of the diffusion coefficient as a function of the cluster size. At high temperatures, the dissociation-recombination (or evaporation-condensation) mechanism becomes more and more important.

4.4 Cluster eccentricity

From the event by event analysis of the cluster configuration, one can study also the temperature dependence of the average cluster shape. This is quantified by the clusters average eccentricity (ε), characterizing the asymmetric nature of the average cluster configuration.

The eccentricity of a cluster configuration is calculated from the coordinates of the component atoms. Our main mathematical tool is the 2×2 eccentricity matrix, E, (4.1a) with elements:

$$E=\begin{pmatrix} E_{xx} & E_{xy} \\ E_{yx} & E_{yy} \end{pmatrix}, \tag{4.1a}$$

$$E_{xx}=\sum_i (X_{MC}-X_i)(X_{MC}-X_i), \qquad E_{xy}=\sum_i (X_{MC}-X_i)(Y_{MC}-Y_i), \tag{4.1b}$$

$$E_{yx}=\sum_i (Y_{MC}-Y_i)(X_{MC}-X_i), \qquad E_{yy}=\sum_i (Y_{MC}-Y_i)(Y_{MC}-Y_i), \tag{4.1c}$$

X_{CM} and Y_{CM} denotes the X, respectively Y coordinates of the clusters CM, X_i and Y_i are the coordinates of i^{th} atom of the cluster. The eccentricity, ε, of a configuration is a scalar, computed from the eigenvalues, λ_1 and λ_2, of matrix E:

$$\varepsilon=\frac{|\lambda_1-\lambda_2|}{\max\{\lambda_1,\lambda_2\}}. \tag{4.2}$$

The eccentricity defined in (4.2) takes values between 0 and 1. For a disc shaped cluster $\varepsilon=0$ and for a linear cluster $\varepsilon=1$.

During our KMC simulations the time-averaged eccentricity of the Pt clusters containing 7, 9, 13, 19, 30 and 37 atoms were studied in a temperature range between $T=300$K and $T=900$K. Results are plotted in Fig. 11. As one would naturally expect, the average eccentricity is always monotonically increasing with temperature. The increased thermal fluctuations will distort the minimum energy disc-like configurations in increasing manner. Fig. 11 indicates also that the considered clusters can be classified into two groups after their $\varepsilon(T)$ trend. The first group contains clusters with eccentricities varying almost linearly as a function of temperature ($N=9$,13, and 30). The second group contains clusters with eccentricity values much smaller at low temperatures and with a non-linear (saturation-like) variation of the eccentricities as a function of temperature ($N=7$, 19 and 37). This second group contains the clusters with closed shell structures.

The eccentricity of the smaller closed shell clusters are higher than the eccentricity of the bigger closed shell configurations. The reasoning is simple: the movement of an atom (a basic event in simulation) will influence in a larger manner the value of the eccentricity for smaller clusters than for the bigger ones. As an example let us consider the case of the Pt_7 and Pt_{19} closed shell clusters. In their basic compact configurations the eccentricities are $\varepsilon=0$ for both of them. Starting from this configuration if an edge atom makes an FCC-HCP diffusion jump the cluster remains the closest possible to disk shape. A simple calculation shows that the new eccentricity values will become $\varepsilon(Pt_7)=0.32$ and $\varepsilon(Pt_{19})=0.09$. For the FCC-FCC jump of an edge atom, the eccentricity will change to $\varepsilon(Pt_7)=0.49$ and $\varepsilon(Pt_{19})=0.13$. In both cases the eccentricity of the $N=7$ cluster is larger.

For closed shell structures one can distinguish three distinct temperature regimes. For temperatures below $T=400$K the edge atoms make short distance jumps, like FCC-HCP.

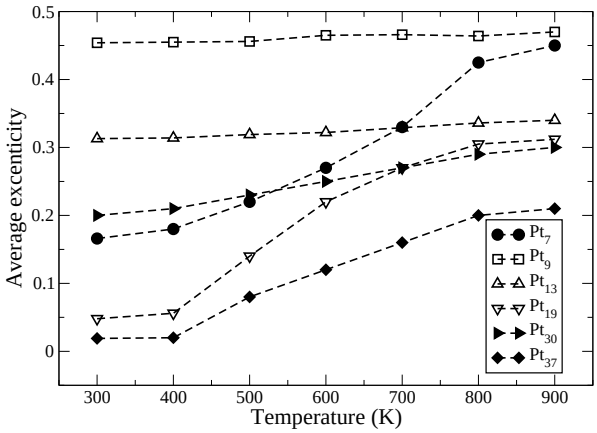

Figure 11: Average eccentricity of the Pt_7, Pt_{13}, Pt_{19}, Pt_{25}, Pt_{30} and Pt_{37} clusters as a function of the system temperature.

In most cases in the next KMC event the atom will jump back, the cluster recombining into the disc shape. The average eccentricity is thus small and increases slowly. For medium temperatures, between $T=400$K and $T=800$K, the distortion increases rapidly with the temperature due to the increasing edge diffusion and dissociation-recombination mechanisms. For temperatures higher than $T=800$K there is a saturating trend in the average eccentricity. Atoms will leave the clusters with a higher probability and their free diffusion on the surface will have no further effect on the cluster eccentricity.

5 Conclusions

Earlier studies [12–14] proved already the applicability of the KMC method for studying several thin-film growth related phenomena: island nucleation and growth, island coalescence, stacking faults related phase boundary motion, co-deposition of several types of atoms, segregation patterns and interesting structures formed during epitaxial growth. In the present study we have used the KMC approach with a realistic interaction potential and barrier heights to study the statistics of the diffusion of Pt clusters on a Pt(111) surface. The results obtained for the value of the diffusion coefficient of clusters up to $N=37$ atoms, their temperature and size dependence of the diffusion coefficient, are all in reasonable agreement with previous experimental and theoretical studies in this system. Our simulation data confirmed the validity of the Arrhenius equation regarding the temperature dependence and the simple $D_0 \sim N^{-1/2}$ scaling assumption for the prefactor. The results also indicate that the single-atom diffusion approximation might not be reasonable for describing the diffusion of small close-shell clusters. In such cases the concerted move of the atoms has to be taken into account.

Visualization of the dynamics, and interpretation of the statistical data, revealed two different mechanisms for the diffusion in the considered model: (i) diffusion of atoms

around and on the periphery of the cluster; (ii) dissociation of the cluster in two or more smaller parts, which can diffuse on the surface and recombine in the original cluster. The jump-size statistics of the cluster's CM and the eccentricity of the cluster's shape, both as a function of temperature and cluster size, offered additional and valuable insides in the diffusion process. A clear picture emerges for the dominant diffusion mechanism. At low temperatures (below $T = 400$K) the periphery diffusion is the leading mechanism, while at high temperatures (above $T = 800$K) the contribution of dissociation-recombination mechanism becomes more and more important.

The KMC method implemented with the EAM potential and the NEB method for determining the energy barrier for diffusion proved to be a fair approximation for studying diffusion of Pt clusters on Pt(111) surfaces.

Acknowledgments

Work supported by contract nr. PNII/ID/PCCE:312/2008.

References

[1] D. Kashchiev, Nucleation: Basic Theory with Applications, Oxford: Division of Reed Educational and Professional Publishing Ltd, 2000

[2] J.-M. Wen, J. W. Evans, M. C. Bartelt, J. W. Burnett and P. A. Thiel, Coarsening mechanisms in a metal film: from cluster diffusion to vacancy ripening, Phys. Rev. Lett., 76 (1996), 652–655.

[3] J. J. De Miguela, A. Sáncheza, A. Cebolladaa, J. M. Gallegoa, J. Ferróna and S. Ferrera, The surface morphology of a growing crystal studied by thermal energy atom scattering (TEAS), Surf. Sci., 189-190 (1987), 1062–1068.

[4] M. Marinica, C. Barreteau, D. Spanjaard and M. Desjonqueres, Influence of short-range adatom-adatom interactions on the surface diffusion of Cu on Cu(111), Phys. Rev. B., 72 (2005), 115402.

[5] S. C. Wang and G. Ehrlich, Diffusion of large surface clusters: direct observations on Ir(111), Phys. Rev. Lett., 79 (1997), 4234–4237.

[6] K. Kyuno and G. Ehrlich, Diffusion and dissociation of platinum clusters on Pt(111), Surf. Sci., 437 (1999), 29–37.

[7] S. C. Wang, U. Krpick and G. Ehrlich, Surface diffusion of compact and other clusters: Irx on Ir(lll), Phys. Rev. Lett., 81 (1998), 4923–4926.

[8] S. Liu, Z. Zhang, J. Nórskov and H. Metiu, The mobility of Pt atoms and small Pt clusters on Pt(111) and its implications for the early stages of epitaxial growth, Surf. Sci., 321 (1994), 161–171.

[9] U. Kurpick, B. Fricke and G. Ehrlich, Diffusion mechanisms of compact surface clusters: Ir_7 on Ir(111), Surf. Sci., 470 (2000), 45–51.

[10] C. L. Liu, J. M. Cohen and J. B. Adams, EAM study of surface self-diffusion of single adatoms of fcc metals Ni, Cu, Al, Ag, Au, Pd and Pt, Surf. Sci., 253 (1991), 334–344.

[11] J. Y. Yang, W. Y. Hu and M. C. Xu, Comparative study of compact hexagonal cluster self-diffusion on Cu(111) and Pt(111), Appl. Surf. Sci., 255 (2008), 1736–1740.

[12] A. F. Voter, Classically exact overlayer dynamics: diffusion of rhodium clusters on Rh (100), Phys. Rev. B., 34 (1986), 6819–6829.
[13] X. P. Wang, F. Xie, Q. W. Shi and T. X. Zhao, Effect of atomic diagonal motion on cluster diffusion coefficient and its scaling behavior, Surf. Sci., 561 (2004), 25–32.
[14] P. M. Agrawal, B. M. Rice and D. L. Thompson, Predicting trends in rate parameters for self-diffusion on FCC metal surfaces, Surf. Sci., 515 (2002), 21–35.
[15] D. Marx and J. Hutter, in: J. Grotendorst (Ed.), Modern Methods and Algorithms of Quantum Chemistry, Proceedings, 2nd Ed. (Julich: John von Neumann Institute for Computing, NIC series), 3 (2000), 329–477.
[16] P. Ruggerone, C. Ratsch and M. S. Scheffer, in: D. A. King and D. P. Woodruff (Eds.), Growth and Properties of Ultrathin Epitaxial Layers (Amsterdam: The Chemical Physics of Solid Surfaces, Elsevier), 8 (1997).
[17] A. F. Voter, in: K. E. Sickafus and E. A. Kotomin (Eds.), Radiation Effects in Solids, Springer (Dordrecht: The Netherlands, NATO Publishing Unit), 2005.
[18] A. B. Bortz, M. H. Kalos and J. L. Lebowitz, A new algorithm for Monte Carlo simulation of Ising spin systems, J. Comput. Phys., 17 (1975), 10–18.
[19] R. Deak, Z. Neda and P. B. Barna, A simple kinetic Monte Carlo approach for epitaxial submonolayer growth, Commun. Comput. Phys., 3 (2008), 822–833.
[20] R. Deak, Z. Neda and P. B. Barna, A novel kinetic Monte Carlo method for epitaxial growth, JOAM., 10 (2008), 2445–2450.
[21] M. Kotrla, J. Krug and P. Smilauer, Submonolayer epitaxy with impurities: kinetic Monte Carlo simulations and rate-equation analysis, Phys. Rev. B., 62 (2000), 2889–2898.
[22] H. Brune, Microscopic view of epitaxial metal growth: nucleation and aggregation, Surf. Sci. Rep., 31 (1998), 121–229.
[23] J. D. Weeks and G. H. Gilmer, Dynamics of crystal growth, Adv. Chem. Phys., 40 (1979), 157–227.
[24] A. F. Voter and J. D. Doll, Transition state theory description of surface self-diffusion: comparison with classical trajectory results, J. Chem. Phys., 80 (1984), 5832–5838.
[25] G. Mills and H. Jónsson, Quantum and thermal effects in H_2 dissociative adsorption: evaluation of free energy barriers in multidimensional quantum systems, Phys. Rev. Lett., 72 (1994), 1124–1127.
[26] G. Henkelman and H. Jónsson, Improved tangent estimate in the nudged elastic band method for finding minimum energy paths and saddle points, J. Chem. Phys., 113 (2000), 9978–9985.
[27] G. Henkelman and H. Jónsson, A dimer method for finding saddle points on high dimensional potential surfaces using only first derivatives, J. Chem. Phys., 111 (1999), 7010–7022.
[28] M. S. Daw and M. I. Baskes, Semiempirical, quantum mechanical calculation of hydrogen embrittlement in metals, Phys. Rev. Lett., 50 (1983), 1285–1288.
[29] H. N. G. Wadley, X. Zhou, R. A. Johnson and M. Neurock, Mechanisms, models and methods of vapor deposition, Prog. Mat. Sci., 46 (2001), 329–377.
[30] X. W. Zhou et al., Atomic scale structure of sputtered metal multilers, Acta. Mater., 49 (2001), 4005–4015.
[31] J. W. Evans, P. A. Thiel and M. C. Bartelt, Morphological evolution during epitaxial thin film growth: formation of 2D islands and 3D mounds, Surf. Sci. Rep., 61 (2006), 1–128.
[32] F. Much and M. Biehl, Simulation of wetting-layer and island formation in heteroepitaxial growth, Europhys. Lett., 63 (2003), 14–20.
[33] Chi-Hang Laml, Chun-Kin Lee and L. M. Sander, Competing roughening mechanisms in

strained heteroepitaxy: a fast kinetic Monte Carlo study, Phys. Rev. Lett., 89 (2002), 216102.
[34] A. Karim et al., Diffusion of small two-dimensional Cu islands on Cu(111) studied with a kinetic Monte Carlo method, Phys. Rev. B., 73 (2006), 165411.
[35] M. J. Mehl and D. A. Papaconstantopoulos, Applications of a tight-binding total-energy method for transition and noble metals: elastic constants, vacancies, and surfaces of monatomic metals, Phys. Rev. B., 54 (1999), 4519–4530.
[36] D. Turnbull, The supercooling of aggregates of small metal particles, Trans. Amer. Inst. Min. Metall. Eng., 188 (1950), 1144–1148.
[37] A. Bogicevic, S. Liu, J. Jacobsen, B. Lundqvist and H. Metiu, Island migration caused by the motion of the atoms at the border: size and temperature dependence of the diffusion coefficient, Phys. Rev. B., 57 (1998), R9459–R9462.
[38] W. W. Pai, A. K. Swan, Z. Zhang and J. F. Wendelken, Island diffusion and coarsening on metal (100) surfaces, Phys. Rev. Lett., 79 (1997), 3210–3213.
[39] G. Rosenfeld, K. Morgenstern, I. Beckmann, W. Wulfhekel, E. Laegsgaard, F. Besenbacher and G. Comsa, Stability of two-dimensional clusters on crystal surfaces: from Ostwald ripening to single-cluster decay, Surf. Sci., 401 (1998), 402–404.